# Using Segmentation Networks on Diabetic Retinopathy Lesions: Metrics, Results and Challenges

Pedro Furtado[a]
*DEI/CISUC, Universidade de Coimbra, Polo II, Coimbra, Portugal*

Keywords: Deep Learning, Segmentation, Medical Images.

Abstract: Deep segmentation networks are increasingly used in medical imaging, including detection of Diabetic Retinopathy lesions from eye fundus images (EFI). In spite of very high scores in most EFI analysis tasks, segmentation measured as precise delineation of instances of lesions still involves some challenges and deserves analysis of metrics and comparison with prior deep learning approaches. We build and confront state-of-the-art deep learning segmentation networks with prior results, showing up to 15 percentage points improvement in sensitivity, depending on the lesion. But we also show the importance of metrics and that many frequently used metrics can be deceiving in this context. We use visual and numeric evidence to show why there is still ample space for further improvements of semantic segmentation quality in the context of EFI lesions.

## 1 INTRODUCTION

Diabetic Retinopathy (DR) is an eye condition related to microvascular changes in the retina that affects people with Diabetes. The changes involve leakage of extra fluid and small amounts of blood in the eye (microaneurysms and hemorrhages) and deposits of cholesterol and other fats (exudates) (Wilkinson, 2003). Figure 1 shows some lesions and some structures on eye fundus image (EFI), where the coloured image indicates the lesions and the optic disk.

The deep segmentation network is a software system inspired in convolution neural networks that uses supervised learning from training images and groundtruths to learn how to segment images in a certain context. These networks are increasingly used in every medical imaging problem with great results when compared to previous alternatives. Figure 2 shows one such network receiving an image as input and outputting a segmentation map that is supposed to classify each pixel as one of a number of classes.

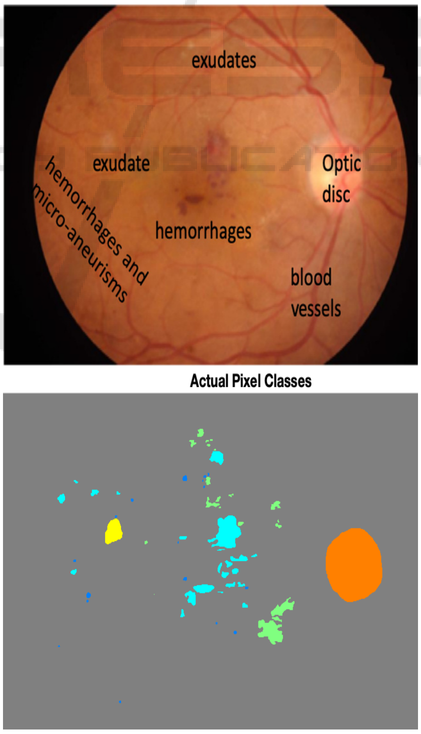

Figure 1: EFI and lesions characteristic of Diabetic Retinopathy.

[a] https://orcid.org/0000-0001-6054-637X

Furtado, P.
Using Segmentation Networks on Diabetic Retinopathy Lesions: Metrics, Results and Challenges.
DOI: 10.5220/0010208501280135
In *Proceedings of the 14th International Joint Conference on Biomedical Engineering Systems and Technologies (BIOSTEC 2021) - Volume 2: BIOIMAGING*, pages 128-135
ISBN: 978-989-758-490-9

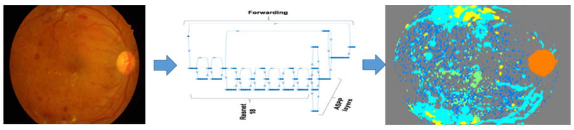

Figure 2: Illustration of the deep segmentation procedure.

The deep segmentation network shown in Figure 2 is made of an encoding and a decoding part. The encoding part is a Convolution Neural Network (CNN), and its function is to extract features from images in the form of a compressed representation of the main features, hence the label "encoding". But while CNNs classify images, segmentation networks classify each individual pixel as belonging to one of a set of classes, a.k.a. semantic segmentation.

Semantic Segmentation, also called scene labeling, refers to assigning a semantic label (e.g. car, people, and road) to each pixel of an image (Yu, 2018). In semantic segmentation each pixel must be assigned the exact class to which it belongs in reality, and groundtruths should be pixelmaps as much as possible, as opposed to coarse regions defined around groups of lesions. In analysis of EFI images, semantic segmentation aims at finding areas and numbers of lesions instances as accurately as possible, as opposed to just detecting if images have lesions of certain types or some regions engulfing sets of lesions.

Recent reviews of EFI analysis, such as in (Qureshi, 2019), (Asiri, 2019), (Raman, 2019) report highest scores (e.g. between 90% and 100%) in most tasks related to analysis of EFI and DR classification. A smaller fraction of the works reviewed there mention lesion segmentation and, as we review in related work section, an even smaller fraction actually evaluate the whole process of segmentation of lesions. For those we have to look into the details to retrieve the actual reported scores. The sensitivities found in those works for one False Positive per Image are in the intervals, for different lesions: hemorrhages HA=47-50%; hard exudates HE=40-57%; soft exudates SE=64-70% and micro-aneurisms MA=7-38%. These values contrast with scores between 90% and 100% for other tasks such as detecting if an image has any lesion of a certain type.

These reported prior works use various CNN-based approaches to EFI analysis. Our purpose in this work is twofold: on one hand we build and compare a state-of-the-art semantic segmentation network (DeepLabV3, FCN, UNET) with those prior works, showing that it improves the results, but on the other hand we also discuss metrics and the need to be careful in the use of metrics when evaluating this kind of systems. Analyzing the quality of segmentation in terms of sensitivity versus false positives we find that our proposed network is quite competitive and overcomes prior work. But at the same time we also reveal the limitations with some frequently applied segmentation metrics in the context of evaluation of segmentation of EFI lesions in general. We discuss limitations of popular metrics that include ROC/AUC, specificity and even sensitivity alone (sensitivity versus false positives, which we use to compare with prior works, does not have the problem) in our context. We show that, from a perspective of evaluation of semantic segmentation, where the class of each individual pixel matters, work is still required to improve the approaches further.

The paper is organized as follows: section 2 contains related work. Section 3 describes the segmentation network we build and propose in this work for the comparisons, and the limitations of some metrics in the context of EFI lesions segmentation is also discussed there. Section 4 contains experimental work and section 5 concludes the paper.

## 2 RELATED WORK

Recent surveys on analysis of Eye Fundus Images (EFI) for diagnosis of Diabetic Retinopathy (DR) and for detection and localization of lesions (Qureshi, 2019), (Asiri, 2019), (Raman, 2019) report scores between 90% and 100% for most tasks, including some mentioning "segmentation" and "localization". The fraction of works reviewed that "segment" lesions include Prentasic et al. (Prentašić,2015), Gondal at al. (Goindal, 2017), Quellec et al. (Quellec, 2017) (exudates, hemorrhages and microaneurisms), Haloi et al. (Haloi, 2015), Van Grinsven et al. (Van Grinsven, 2016), Orlando et al. (Orlando, 2018) and Shan et al. (Shan, 2016) (microaneurisms, hemorrhages or both). From those, a considerable number are classifiers of small windows. That is the case of Prentasic et al. (Prentašić,2015), Haloi et. al. (Haloi, 2015), Van Grinsven (Van Grinsven, 2016), and Shan et al. (Shan, 2016), which are classification CNNs that classify small square windows around potential lesions. These works achieve high classification scores, but they do not segment the lesions, instead they classify small windows. For instance, (Prentašić,2015) proposes applying a simple CNN classifier to each pixel by obtaining a small window around it, and achieves a classification score of 77% sensitivity for exudates. Not only the sensitivity is lower than 90 to 100% and target only exudates, as also for training and evaluation the authors collect windows statically, taking all the exudate pixels as positive samples and the same amount of pixels randomly sampled among all non-exudate pixels but without repetition. The approach does not deal with the difficulty of scaling to classify all pixels in an EFI and realtime operation, a difficult issue because the classifier has to be applied to each pixel. More generically, it is not clear how to scale approaches classifying small windows around pixels to realtime semantic segmentation of lesions.

Other related works do segment lesions, e.g. Gondal at al. (Gondal, 2017), Quellec et al. (Quellec, 2017) are two variations of DR classifiers (classification of EFI images as DR or not), that at the same time up-sample and extract heatmaps to get the positions of lesions. Orlando (Orlando, 2018) uses a different approach that combines DL with image processing to find candidate regions. These works do include evaluation of the quality of segmentation of lesions, using a criterion of overlap of segments. They reported the following sensitivities for segmentation of lesions (for 1 false positive per image=FPI): Quellec (Quellec, 2017) (HA=47%; HE=57%; SE=70% and MA=38%), Gondal (Gondal, 2017) (HA=50%; HE=40%; SE=64% and MA=7%) and Orlando (Orlando, 2018) (HA:50%, MA: 30%). These scores illustrate the fact that segmenting the lesions does not result in scores near to 100%. Also important, it must be noted that a “relaxed” connected components evaluation criteria is used in those works (described for instance in (Zhang, 2014)), where a threshold of partial overlap between found segments and groundtruth regions is sufficient for considering a match. The connected components criteria, described for instance in Zhang’s work (Zhang, 2014), considers a match if an overlap of 20% (or another threshold) between found segments and groundtruth regions exists. The groundtruths of the datasets themselves are frequently large coarse regions defined around groups of lesions (e.g. datasets Diaret (Kälviäinen, 2007)] or e-ophtha (Erginay, 2008)). We believed that a state-of-the-art deep learning segmentation network (DeepLabV3) can do better than many prior approaches, such as (Gindal, 2017), (Quellec, 2017), (Orlando, 2018). For that reason, we created the setup and compared the approaches.

Some frequently used metrics are also an important detail in this context (Tiu, 2019), (Csurka, 2013) and in particular class imbalance can bias the evaluation scores. Zhang (Zhang, 2014) mentions that, “given that the classes are clearly unbalanced, TP, FN and FP are in practice negligible with respect to TN, therefore computing the specificity, i.e. TN/(FP+TN), and therefore ROC (Receiver operating characteristic) curve does not seem appropriate”. For that reason we pay a special attention to how metrics should be used in our study. In that respect we both discuss metrics and in the experimental work we include a section revealing the false positives-related limitations of current approaches that are exposed by use of some metrics and/or visual inspection.

There exist some very popular segmentation networks. The Fully Convolutional Network (FCN) (Long, 2015) uses a CNN to encode (typicaly a VGG16 (Simonyan, 2014)), replacing the final fully connected layers by convolutional layers with large receptive fields, and adds up-sampling layers based on simple interpolation filters. The FCN we use in this paper has around 50 layers. We would also mention the use of forwarding paths. Ronneberger (Ronneberger, 2015) proposed the U-Net, a DCNN especially designed for segmentation of biomedical images (around 75 layers). The architecture consists of “a contracting path to capture context” and a “symmetric expanding path that enables precise localization”. The network beat other competitors in the ISBI challenge for segmentation of neuronal structures in electron microscopic stacks. Finally, the DeepLabV3 network (Chen, 2017) that we experiment with uses Resnet-18 encoder and applies some new techniques to improve the quality, including Atrous Spatial Pyramid Pooling (ASPP) (Lin, 2017), capturing objects at multiple scales, and Conditional Random Fields (CRF) for improved localization of object boundaries using probabilistic graphical models. We obtained some of the best results using this network (Porwal, 2019).

# 3 SEGMENTATION NETWORKS AND METRICS

## 3.1 Segmentation Networks

As already mentioned before, segmentation networks have two well distinguished parts, the encoder, most frequently an existing CNN encoding architecture, and a decoder that reinstates the full image size, and the pixel classifier layer that assigns a score for each class to each pixel. DeepLabV3, with a rough sketch shown in Figure 3, is a very successful segmentation network. Our design for DeepLabv3 shown in Figure 3 includes well-known Resnet-18 CNN classification network as encoder and benefits from the innovations that include Atrous Spatial Pyramid Pooling (ASPP) (Lin, 2017), which enables better segmentation at multiple scales, and Conditional Random Fields (CRF), which improve definition of contours in final result. The network accepts as input the full EFI image and outputs the classification for each individual pixel as belonging to a specific lesion or not. The fact that it classifies all individual pixels end-to-end at the same time in one pass (typically taking a few milliseconds to classify all pixels at once) makes it the perfect tool for segmentation, as compared with any CNN that would output an accurate classification of a single pixel but would not scale well. Since backpropagation learning is applied end-to-end with segmentation masks as targets, the network actually learns how to segment images based on the groundtruths. DeepLabV3 is about 100 layers deep. Figure 4 shows the architecture of FCN, another well-known network architecture that uses VGG16 instead and has a total of about 50 layers.

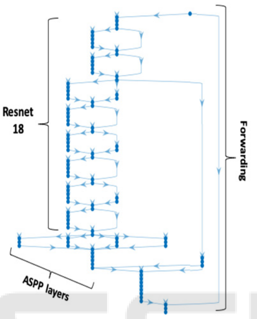

Figure 3: DeepLabV3.

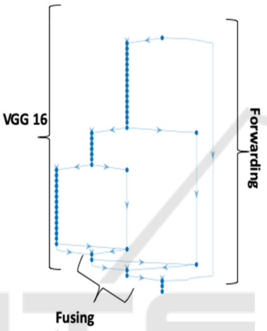

Figure 4: FCN.

## 3.2 Limitations of Metrics

Most works on EFI analysis, and in particular in segmentation of lesions in EFI images, frequently report metrics such as sensitivity, ROC curves and AUC. But in some circumstances, those metrics can bias the analysis in the context that is being considered. As we already reviewed in the related work, Zhang (Zhang, 2014) mentions: “given that the classes are clearly unbalanced, TP, FN and FP are in practice negligible with respect to TN, therefore computing the specificity, i.e. TN/(FP+TN), and therefore ROC (Receiver operating characteristic) curve does not seem appropriate”. The TN mentioned by Zhang refers to the true negatives represented by the background, which composes 90 to 95% of all pixels in the EFI. The background is much easier to segment than the rest of the objects because it is fairly constant and huge, and the problem is that such huge number may mask the real quality of segmentation of lesions. Looking at the formulas of some popular metrics we can see that specificity and false positive rate (FPR) will both score very well “always” in the EFI segmentation context due to that bias, and therefore ROC curves and AUC using FPR are also problematic:

$$specificity = \frac{TN}{TN + FP}$$

$$false\ positive\ rate\ (FPR) = \frac{FP}{FP + TN}$$

ROC: a function usually based on TPR vs FPR

There is also a potential limitation with the metric sensitivity, also known as recall or TPR if it is used alone:

$$sensitivity = recall = TPR = \frac{TP}{TP + FN}$$

In this case the limitation is that it does not consider false positives (FP), meaning that a situation with a huge number of FP could still have high sensitivity. FPs are common because background pixels are sometimes classified as a lesion since parts of the background can resemble a lesion in colour or other details. Evaluations using sensitivity versus false positives (FP) solve this problem, as also does the use of IoU (intersect-over-the-union) or the pair recall + precision, because in those cases FPs are considered:

$$precision = \frac{TP}{TP + FP}$$

$$IoU = \frac{TP}{TP + FN + FP}$$

The last part of our experimental work concerns precisely the analysis of the FP problem, revealing that there are still important limitations of the approaches due to a significant amount of FP. Future work should try to handle that problem.

# 4 EXPERIMENTAL RESULTS

For this investigative work we work with two datasets. On one hand we use the publicly available dataset IDRID dataset (Porwal, 2019), with 83 Eye Fundus Images (EFI) and groundtruth pixelmaps, where most images have a large number of instances of each specific lesion. To increase the variety and size of the training data we introduced data augmentation in the training process, with random translations of up to 10 pixels. For the comparison with prior works to be based on the same dataset and evaluation approach, we use DIARET-DB1 dataset (Kauppi, 2007). DIARET-DB1 consists of 89 color fundus photographs collected at the Kuopio

University Hospital, in Finland (Kauppi et al., 2007). Images were captured with the same fundus camera, a ZEISS FF450plus digital camera with a 50-degree field-of-view. Images all have a definition of 1500 x 1152 pixels. Independent markings were obtained for each image from four medical experts. The experts were asked to manually delineate the areas containing microaneurysms (or 'small red dots'), hemorrhages, hard exudates and cotton wool spots (a.k.a 'soft exudates') and to report their confidence (< 50 %, ≥ 50 %, 100 %) for each segmented lesion.

We initially obtain performance scores for DeepLabV3, FCN and even U-Net to choose DeepLabV3 as the main contender for comparison with prior Works. Then we report the results of DeepLabV3 compared to results with prior works (Gondal, 2017), (Quellec, 2017), (Orlando,2018) regarding quality of segmentation. After showing that DeepLabV3 improves compared with those approaches, we use visual and metric approaches on the first dataset (IDRID) to show the limitations related to FP and the need for more work improve the approaches further.

For all networks the SGDM learning optimization function was used, with learning rate 0.005 that allowed the networks to converge to a classification of all lesions. Training used 300 epochs, since all networks would stabilize much before that, minibatch sizes of 32, momentum of 0.9. In terms of hardware, we used a machine running windows 10. The hardware was an intel i5, 3.4 GHz, 16 GB of RAM 1TB SSD disk. A GPU was added to the PC, consisting of an NVIDEA GForce GTX 1070 GPU (the GTX 1070 has a Pascal architecture and 1920 cores, 8 GB GDDR5, with memory speed of 8 Gbps).

Our first experiment intended to pick the segmentation network that would exhibit best results using IDRID. Figure 5 compares three networks. FCN had very good accuracy and IoU (90%, 88%), DeepLabV3 was also quite good, always > 75%, and both exhibited improvements over U-Net. We will show later on (Table 3) that IoU scores per lesion are much worse than these metrics shown in Figure 5, which is related to the need for a careful interpretation of metrics. Accuracy measures the fraction of pixels that were classified well versus all pixels, and weighted IoU measures the degree of correct overlap of regions. These metrics usually score very high when averaged over all pixels simply because the background is huge and most of it is well segmented because it is fairly constant (eye fundus).

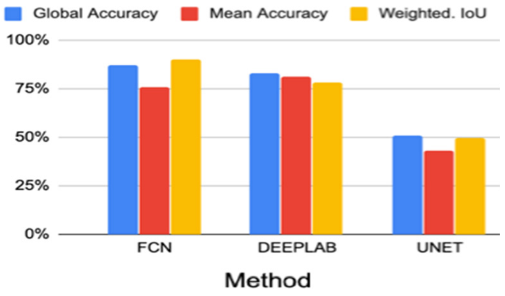

Figure 5: Comparing FCN, DeepLabV3 and U-Net.

## 4.1 Comparing Lesion and Image-Level Sensitivities to Prior Works

Table 1 shows the results we obtained concerning the comparison of lesion-level sensitivities between our approach and those in (Gondal, 2017) and in (Quellec, 2017). These results were obtained using the connected components model of evaluation (Zhang, 2014) with similar conditions as used in the compared works. The sensitivities are measured against the number of false positives per image (FPI), and both should be considered in the analysis of results. Note that we used the approach in (Quellec, 2017) where FPIs can differ because they are obtained against the class classification threshold (0 to 1). Since only thresholds in the interval 0.1 and 0.9 with 0.1 steps are tested, only some values for FPI are obtained, and from those, one is chosen that allows easy comparison, as much as possible.

In general these results show that sensitivities vary significantly between works and varied between 50 and 87% for HE, 47 and 94% for HE, 71 and 90% for SE and 21 and 61% for RSD, also depending on the number of FPI to consider.

They show that DeeplabV3 actually improves scores for most lesions, i.e. for HA, HE and SE, while for MA the results seem worse than (Orlando, 2018) but inline with the results of the remaining prior work compared.

Table 2 compares image-level detection of lesions for referral, DeepLabV3 ranks first in HA and SE and also ranks well in HE and MA. We can also see that this is a quite easy problem for any technique, since the objective is only to tell whether there is any lesion of a certain type in the whole EFI image, without the need to locate any precisely.

Table 1: Comparing lesion-level sensitivities.

| **Method** | **Hemorrhages** | | **Hard Exudates** | | **Soft Exudates** | | **RSD (micro-aneurisms)** | |
|---|---|---|---|---|---|---|---|---|
| | **SE%** | **FPs/I** | **SE%** | **FPs/I** | **SE%** | **FPs/I** | **SE%** | **FPs/I** |
| (Quellec, 2017) | 71 | 10 | 80 | 10 | 90 | 10 | 61 | 10 |
| Gondal, 2017) | 72 | 2.25 | 47 | 1.9 | 71 | 1.45 | 21 | 2 |
| (Orlando, 2018) | 50 | 1 | | | | | 50 | 1 |
| Ours | **87** | 10 | **94** | 2.76 | **87.5** | 3.92 | 48 | 6.4 |

Table 2. Image-level sensitivities.

| **Method** | HA | HE | SE | MA |
|---|---|---|---|---|
| (Zhou, 2016) | 94.4 | - | - | - |
| (Liu, 2017) | - | 83 | 83 | - |
| (Haloi, 2015) | - | **96.5** | - | - |
| (Mane, 2015) | - | - | - | **96.4** |
| (Gondal, 2017) | 97.2 | 93.3 | 81.8 | 50 |
| Ours | **100** | 90 | **87.5** | 71 |

## 4.2 Limitations Revealed using Semantic Segmentation Metrics

In spite of good comparative results when measured using the connected components model (Zhang, 2014) that is used in most works on segmentation of lesions in EFI, we also found that a large number of false positives appears if we try to obtain higher scores for lesions (sensitivities), especially apparent if we evaluate in the perspective of semantic segmentation. While in the connected component model overlaps between segments are evaluated and 50%, 20% or any overlap at all are considered matches, in "semantic segmentation" each pixel must be assigned the exact class to which it belongs and groundtruths should be pixelmaps with, as much as possible, the exact class of each pixel. Since the groundtruths of the IDRID dataset (Porwal, 2019) are near to this concept where each pixel is assigned its class, the next experiment evaluates based on this principle. Figure 6 shows, on the left, the groundtruth segments superimposed on the image, for FCN and for DeepLabV3, and on the right the corresponding segmentations. Many FP are apparent on the right, more so in DeepLabV3.

Taking the segmentation masks of the same image on FCN, Figure 7 shows, on the left image, the real groundtruth mask for the lesions and optic disk, and the right image shows lesions and optic disk pixels that were not detected. We can see that only a very small fraction of all lesions (which corresponds to around 2.2%) were undetected, which is a very good result. This corresponds to high sensitivity (SE).

If we analyze IoU of each class (each lesion plus the optic disk and the background), it reveals the deficiencies of segmentation outputs. Those results shown in Table III reveal that the background and optic disk have high IoU scores, but the lesions, have low IoU scores, between 19 and 38%.

This is also seen visually in Figure 8, showing the groundtruth labels (a) and the background false positives (b), which are background pixels classified as lesions. The total area of those false positives is 8% of all image pixels or around 100% of all lesions plus optic disk pixels. This agrees with the large amounts of FP previously in the outputs of segmentation in figure 6. The conclusion is that more work is necessary in the future to improve and filter out false positives.

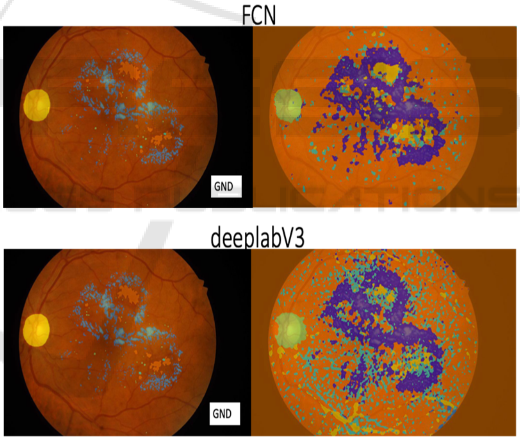

Figure 6: Comparing groundtruths with outputs: Deeplab and FCN.

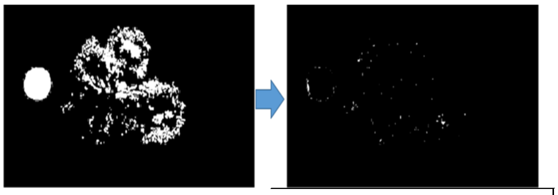

(a) Groundtruth

(b) Undetected Lesions (2.2%)

Figure 7: FCN detections of lesions.

### 4.3 Conclusions from Experiments

It is a common misconception that segmentation of eye fundus lesions already achieves almost 100% quality, and this misconception is supported by the way metrics are used and also by the interpretation of the task. One example is to consider partial overlaps (e.g. > 10%) as detected lesion, versus measuring precise degree of overlap (semantic segmentation). Our experiments show that a simple segmentation network scores very high and higher than prior work in the tasks using those loose interpretations, but still has serious difficulties correctly segmenting small lesions using the semantic segmentation interpretation (e.g. 21 to 32% IoU for small lesions). As a conclusion, further work is necessary in the future to improve the approaches.

Table 3: Per-class IoU.

| Class | IoU FCN | IoU Deeplab |
|---|---|---|
| Background | 88 | 83 |
| OpticDisc | 75 | 70 |
| SoftExudates | 35 | 32 |
| Haemorrhages | 38 | 32 |
| HardExudates | 26 | 26 |
| Microaneurs | 19 | 21 |

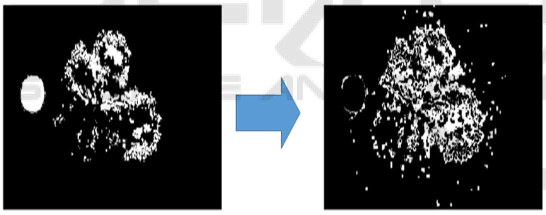

(a) Groundtruth

(b) FP~=100% of lesions area

Figure 8: FCN false positives.

## 5 CONCLUSIONS

In this work we have studied the problem of accurate segmentation of Eye-Fundus-Lesions. We have proposed and evaluated carefully the use of deep segmentation networks, in particular DeepLabV3 and FCN, concluding that the proposed approach improves when compared with previous work. But we also highlighted some limitations of current approaches, which are revealed mostly if we evaluate the quality of semantic segmentation and use false positives revealing metrics, such as IoU. We also explain why we need to be careful with some metrics, such as specificity, ROC or AUC in the context of segmentation of lesions in EFI, and what sensitivity alone does not reveal. In our future work we will experiment more with loss functions and filtering out false positives as some post-processing step, but also improvements in architectures to deal with small lesions.

## ACKNOWLEDGMENTS

We have used datasets (Porwal, 2019) (Kauppi, 2007) in our experimental work, we thank the organizers of those datasets for their availability.

## REFERENCES

Asiri, N., Hussain, M., Al Adel, F., & Alzaidi, N. (2019). Deep learning based computer-aided diagnosis systems for diabetic retinopathy: A survey. Artificial intelligence in medicine.

Chen, L. C., Papandreou, G., Kokkinos, I., Murphy, K., & Yuille, A. L. (2017). Deeplab: Semantic image segmentation with deep convolutional nets, atrous convolution, and fully connected crfs. IEEE transactions on pattern analysis and machine intelligence, 40(4), 834-848.

Csurka C., Perronnin (G. and F.), "What is a good evaluation measure for semantic segmentation?," Proceedings of the British Machine Vision Conference , 32.1–32.11. (2013).

Decencière et al.. Feedback on a publicly distributed database: the Messidor database. Image Analysis & Stereology, v. 33, n. 3, p. 231-234, aug. 2014. ISSN 1854-5165.

Erginay, A., Chabouis, A., Viens-Bitker, C., Robert, N., Lecleire-Collet, A., Massin, P., Jun 2008. OPHDIAT: quality-assurance programme plan and performance of the network. Diabetes Metab 34 (3), 235–42.

Giancardo, L., Meriaudeau, F., Karnowski, T., Li, Y., Garg, S., Tobin, K., Chaum, E., 2012. Exudate-based diabetic macular edema detection in fundus images using publicly available datasets. Med. Image Anal. 16 (1), 216–226.

Gondal, W. M., Köhler, J. M., Grzeszick, R., Fink, G. A., & Hirsch, M. (2017, September). Weakly-supervised localization of diabetic retinopathy lesions in retinal fundus images. In 2017 IEEE international conference on image processing (ICIP) (pp. 2069-2073).

Haloi, M. (2015). Improved microaneurysm detection using deep neural networks. arXiv preprint arXiv:1505.04424.

Kälviäinen, R. V. J. P. H., & Uusitalo, H. (2007). DIARETDB1 diabetic retinopathy database and evaluation protocol. In Medical Image Understanding and Analysis (Vol. 2007, p. 61).

Kauppi, T., Kalesnykiene, V., Kamarainen, J.-K., Lensu, L., Sorri, I., Raninen, A., Voutilainen, R., Pietila¨, J., Ka¨lvia¨inen, H., Uusitalo, H., 2007. The DI-ARETDB1 diabetic retinopathy database and evaluation protocol. In: Proc BMVC. Warwik, UK.

Lin, T. Y., Dollár, P., Girshick, R., He, K., Hariharan, B., & Belongie, S. (2017). Feature pyramid networks for object detection. In Proceedings of the IEEE Conference on Computer Vision and Pattern Recognition (pp. 2117-2125).

Liu Q., Zou B., Chen J., Ke W., Yue K., Chen Z., and Zhao G., “A location-to-segmentation strategy for automatic exudate segmentation in colour retinal fundus images,” Computerized Medical Imaging and Graphics, vol. 55, pp. 78–86, 2017.

Long, J., Shelhamer, E., & Darrell, T. (2015). Fully convolutional networks for semantic segmentation. In Proceedings of the IEEE conference on computer vision and pattern recognition (pp. 3431-3440).

Mane V., Kawadiwale R., and Jadhav D., “Detection of red lesions in diabetic retinopathy affected fundus images,” in IEEE Inter- national Advance Computing Conference (IACC), 2015, pp. 56–60.

Orlando, J. I., Prokofyeva, E., del Fresno, M., & Blaschko, M. B. (2018). An ensemble deep learning based approach for red lesion detection in fundus images. Computer methods and programs in biomedicine, 153, 115-127.

Porwal, Prasanna, S. P. R. K. M. K. G. D. V. S. and Meriaudeau, F., “Indian diabetic retinopathy image dataset (idrid).,” IEEE Dataport. (2019).

Prentašić, P., & Lončarić, S. (2015). Detection of exudates in fundus photographs using convolutional neural networks. In 2015 9th International Symposium on Image and Signal Processing and Analysis (ISPA) (pp. 188-192).

Quellec, G., Charrière, K., Boudi, Y., Cochener, B., & Lamard, M. (2017). Deep image mining for diabetic retinopathy screening. Medical image analysis, 39, 178-193.

Qureshi, I., Ma, J., & Abbas, Q. (2019). Recent development on detection methods for the diagnosis of diabetic retinopathy. Symmetry, 11(6), 749.

Raman, R., Srinivasan, S., Virmani, S., Sivaprasad, S., Rao, C., & Rajalakshmi, R. (2019). Fundus photograph-based deep learning algorithms in detecting diabetic retinopathy. Eye, 33(1), 97-109.

Ronneberger, O., Fischer, P., & Brox, T. (2015). U-net: Convolutional networks for biomedical image segmentation. In International Conference on Medical image computing and computer-assisted intervention (pp. 234-241). Springer, Cham.

Salehi, S., Erdogmus D., and Gholipour A., “Tversky loss function for image segmen- tation using 3d fully convolutional deep networks,” in International Workshop on Machine Learning in Medical Imaging, 379–387, Springer (2017).

Sánchez, C., Niemeijer, M., Išgum, I., Dumitrescu, A., Suttorp-Schulten, M., Abràmoff, M., van Ginneken, B., 2012. Contextual computer-aided detection: Improving bright lesion detection in retinal images and coronary calcification identification in ct scans. Med. Image Anal. 16 (1), 50–62.

Shan, J., & Li, L. (2016). A deep learning method for microaneurysm detection in fundus images. In 2016 IEEE First International Conference on Connected Health: Applications, Systems and Engineering Technologies (CHASE) (pp. 357-358).

Simonyan, Karen, and Andrew Zisserman. "Very deep convolutional networks for large-scale image recognition." arXiv preprint arXiv:1409.1556 (2014).

Tiu E., “Metrics to evaluate your semantic segmentation model. (2019). [URL Accessed 8/2019]. URL: https://towardsdatascience.com /metrics-to-evaluate-your-semantic-segmentation-model-6bcb99639aa2.

Van Grinsven, M. J., van Ginneken, B., Hoyng, C. B., Theelen, T., & Sánchez, C. I. (2016). Fast convolutional neural network training using selective data sampling: Application to hemorrhage detection in color fundus images. IEEE transactions on medical imaging, 35(5), 1273-1284.

Wilkinson C., Ferris F., Klein R.,et al. (2003). Proposed international clinical diabetic retinopathy and diabetic macular edema disease severity scales, in Ophthalmology110(9),1677–1682 (2003).

Yu, H., Yang, Z., Tan, L., Wang, Y., Sun, W., Sun, M., & Tang, Y. (2018). Methods and datasets on semantic segmentation: A review. Neurocomputing, 304, 82-103.

Zhang, X., Thibault, G., Decencière, E., Marcotegui, B., Laÿ, B., Danno, R. & Chabouis, A. et al. (2014). Exudate detection in color retinal images for mass screening of diabetic retinopathy. Medical image analysis, 18(7), 1026-1043.

Zhou L., Li P., Yu Q., Qiao Y., and Yang J., “Automatic hemorrhage detection in color fundus images based on gradual removal of vascu- lar branches,” in IEEE International Conference on Image Processing (ICIP), 2016, pp. 399–403.